University of Baghdad
College of Engineering
JOURNAL OF ENGINEERING

Journal of Engineering

journal homepage: www.jcoeng.edu.iq

Volume 32 Number 11 November 2026

IFT–Wettability Interplay and Force-Regime Transition in Chemical EOR: A Mechanistic SI/FI Diagnostic Approach

Faaiz Al-Shajalee [1,*], Hussein H. Hussein [2], Ahmad Sari [3], Lionel Esteban [4], Haider A. Falih Al-Tarim [5], Nurudeen Yekeen [6]

[1] Department of Petroleum Engineering, College of Engineering, University of Kirkuk, Kirkuk, Iraq
[2] Department of Petroleum Engineering, College of Engineering, University of Baghdad, Baghdad, Iraq
[3] Monadelphous, Mining & Minerals Northwest Region, Perth, Western Australia, Australia
[4] Commonwealth Scientific Industrial Research Organisation (CSIRO), Perth, Western Australia, Australia
[5] Oil Exploration Company, Ministry of Oil, Baghdad, Iraq
[6] School of Engineering, Edith Cowan University, Joondalup, Western Australia, Australia

ABSTRACT

Despite the crucial role of enhanced oil recovery (EOR) in meeting rising energy demands, interpretation of chemical EOR (CEOR) performance is limited by reliance on interfacial tension (IFT) and contact angle (CA) data. Most studies correlate IFT and CA with core flooding results, masking the contribution of capillary and gravity forces. The study introduces a force-isolation workflow that distinguishes capillary-, viscous-, and gravity-governed recovery by combining spontaneous imbibition (SI) and forced imbibition (FI) experiments conducted on clay-rich Bandera Gray sandstone cores. The key novelty is a modified Amott cell that applies controlled hydraulic pressure heads (10–30 cm) during the FI experiment, which allows measuring the lowest pressure to trigger oil displacement in every fluid system. Four injection systems—high-salinity (HS) brine, low-salinity (LS) brine, an anionic surfactant (sodium lauryl sulfate, SLS), and a cationic surfactant (cetyltrimethylammonium bromide, CTAB)—are selected to induce interfacial conditions. SLS generates high capillary pressure and a near-zero contact angle, promoting capillary-assisted viscous FI at the lowest pressure threshold, achieving 41% SI recovery and an SI/FI ratio of ~80%. By contrast, CTAB produces a low IFT but insufficient capillary pressure, resulting in gravity-driven SI with 5% recovery and viscous-dominated FI, with an SI/FI ratio of ~9%. The brine systems exhibit viscous-assisted capillary recovery, requiring the highest entry pressure. The SI/FI ratio classifies the force regimes, confirming that capillary support governs mobility control under SI and FI conditions. This force-regime approach provides a more reliable basis for CEOR formulation design than IFT and CA screening alone.

Keywords: Capillary forces, Forced imbibition, Interfacial tension, Spontaneous imbibition, Wettability alteration.

*Corresponding author
Peer review under the responsibility of University of Baghdad.
https://doi.org/10.31026/j.eng.2026.11.02
This is an open access article under the CC BY 4 license (http://creativecommons.org/licenses/by/4.0/).
Article received: 20/07/2026
Article revised: 29/09/2026
Article accepted: 02/10/2026
Article published: 01/11/2026

1. INTRODUCTION

Enhanced oil recovery (EOR) is necessary in order to meet the growing energy **(Ali et al., 2017; Awan and Kirmani, 2025; Chai et al., 2024; Chaturvedi et al., 2024; Haghighi et al., 2020)**. In this context, chemically engineered displacing solutions have been shown to be among the most effective ways for detaching and mobilizing trapped oil in hydrocarbon reservoirs **(Al-Anssari et al., 2021; Ali et al., 2015; Jha et al., 2019)**. The most common mechanisms proposed in the literature for chemical enhanced oil recovery (CEOR) involve modifying fluid–fluid and fluid–rock interactions (i.e., altering the interfacial tension (IFT) and rock wettability) **(Al-Anssari et al., 2018; Al-Shajalee et al., 2025; Dashtaki et al., 2020; Fattahi et al., 2023; Hosseini et al., 2019)**. However, while numerous studies have reported EOR with reductions in the IFT and contact angle (CA), other investigations have found no conclusive evidence to support this relationship **(Deng et al., 2023b; Kamal et al., 2017; Wang et al., 2011; Xu et al., 2019; You et al., 2018)**. For instance, **(Xu et al., 2019)** documented that interfacial tension (IFT) decrease and wettability change (WA) had opposing and coupled effects on capillary-based recovery, where too much IFT decrease dilutes the positive capillary pressure that is produced by WA **(Xu et al., 2019)**. Similarly, **(Deng et al., 2023b)** have studied the relative roles of IFT reduction and WA in different residual oil types and they have concluded that ultralow IFT may inhibit recovery in oil-wet systems that are then switched to water-wet conditions, as the resulting capillary force, which is now a positive driving force, is lowered by the lowered interfacial energy **(Deng et al., 2023a)**.

These contradictory findings highlight the fact that both IFT reduction and WA are not dependable predictors of recovery performance. Therefore, the influence of IFT and CA reduction on oil recovery remains a subject of debate **(Azad, 2021; Deng et al., 2023a)**. Moreover, this debate continues because most researchers have attempted to address the challenge by directly correlating the IFT and CA with forced imbibition (FI) or spontaneous imbibition (SI) results only **(Deng et al., 2023b; Deng et al., 2021; Kamal et al., 2017; Rahevar et al., 2023; Xu et al., 2019)**. It is important to note that most mechanistic studies of the interfacial-tension-wettability interaction have been conducted at the carbonate concentration **(Deng et al., 2021; Rostami Ravari et al., 2011)** or at the pore scale through micro models visualization **(Zhang et al., 2021)**, and therefore, the core-scale behavior of the interplay in clay-rich sandstone reservoirs is relatively under investigated.

A further dimension of this debate concerns the role of surfactant chemistry. Cationic surfactants such as CTAB alter wettability in carbonate systems via ion-pair formation with adsorbed organic carboxylates **(Deng et al., 2021; Kamal et al., 2017)**, but their comparatively greater IFT reduction relative to wettability modification in sandstone suppresses capillary-driven imbibition **(Rostami Ravari et al., 2011; Xu et al., 2019)**. By contrast, anionic surfactants such as SLS generate stronger capillary pressure through aggressive wettability alteration while maintaining moderate IFT **(Kamal et al., 2017; Wang et al., 2011)**, and low-salinity brine promotes wettability alteration through electrical double layer expansion without significant IFT reduction **(Rahevar et al., 2023; Xu et al., 2019)** — making it a useful baseline for isolating interfacial charge effects from surfactant-induced IFT reduction. The transition between capillary-, gravity-, and viscous-dominated recovery regimes has been documented by **(Rostami Ravari et al., 2011)** in carbonate cores, where three distinct recovery stages were identified and shown to shift systematically with IFT, and the SI/FI ratio has been proposed as a diagnostic tool to quantify these force contributions **(Aslanidis et al., 2022; Liu et al., 2025; Rostami Ravari et al., 2011)**.

However, these frameworks have not been combined with quantitative capillary pressure calculations into a unified force-regime classification for CEOR systems in clay-rich sandstone.

However, core flooding alone cannot collectively evaluate the forces responsible for CEOR because, in this method, oil recovery is dominated by the viscous force, while the impacts of capillary and gravity forces are negligible **(Deng et al., 2021). T**he viscous force relates more to factors such as viscosity and injection velocity, while capillary force is directly influenced by the IFT and CA. As such, the IFT and CA may not necessarily correlate with core flooding results **(Deng et al., 2023b; Deng et al., 2021; Kamal et al., 2017; Wang et al., 2011; Xu et al., 2019)**. In this respect, an SI test can serve two important objectives. Firstly, it can isolate the impact of capillary and gravity forces by eliminating the influence of viscous forces, thereby allowing for a more direct assessment of the IFT and CA **(Deng et al., 2021; Xu et al., 2019)**. Secondly, it can provide a mechanistic understanding via visual documentation of oil expulsion from core samples **(Deng et al., 2021; Gupta et al., 2020; Rostami Ravari et al., 2011; You et al., 2018)**. While recent studies have proposed SI/FI comparisons as a means of distinguishing force contributions in tight formations **(Aslanidis et al., 2022; Liu et al., 2025)**, a systematic workflow that links quantitative capillary pressure, IFT, CA, and the SI/FI ratio into a unified force-regime classification has not been established for water-wet sandstone systems under CEOR conditions. Furthermore, existing FI studies typically apply high pump-driven pressures that exceed the threshold at which oil begins to mobilize, thereby obscuring the minimum viscous force required to initiate displacement. To the best of the authors' knowledge, no study has employed a low-pressure, gravity-head forced imbibition setup — as used here — to systematically identify the entry pressure threshold for each CEOR fluid as a direct function of its interfacial properties.

However, despite the reported three-stage SI recovery behavior, i.e., the transition of capillary-dominated to combined capillary-gravity to gravity-dominated drainage, in carbonate cores **(Rostami Ravari et al., 2011)**, and the findings of pore-scale micromodel experiments, showing that wettability change controls early-stage recovery and interfacial tension reduction controls late-stage recovery **(Zhang et al., 2021)**, these insights have not been systematically translated into a core-scale diagnostic framework applicable to sandstone. Unlike previous CEOR studies that correlate the IFT and CA with either FI or SI individually, the present study introduces a diagnostic force-isolation workflow that systematically links IFT, wettability alteration, and oil recovery through combined SI, FI, and SI/FI analysis in a clay-rich Bandera Gray sandstone. Central to this workflow is a modified Amott cell that applies controlled, low-magnitude hydraulic pressure heads (10–30 cm), enabling the minimum entry pressure required to mobilize trapped oil to be determined for each fluid system — a measurement that directly quantifies the threshold viscous force and its dependence on the interfacial conditions induced by the chemical formulation. By classifying recovery behavior into capillary-, gravity-, and viscous-dominant regimes, the proposed SI/FI ratio provides a mechanistic interpretation framework that explains why a low IFT does not always translate into capillary-driven recovery. This way, the study extends the existing understanding of force regimes by shifting the carbonate and pore-scale approaches to a sandstone system, thus providing a quantitative basis, based on the calculation of capillary pressure, to test CEOR equations. This approach establishes force-regime classification as a more reliable basis for CEOR formulation design compared to IFT and wettability measurements alone. Based on this theoretical understanding, an experimental workflow is designed in order to isolate and evaluate force contributions.

Four different displacing solutions are used, including low-salinity (LS) brine, high-salinity (HS) brine, HS brine with a cationic surfactant, and HS brine with an anionic surfactant. Each fluid is expected to have a distinguishable effect on the physicochemical interactions at the rock–fluid and fluid–fluid interfaces, thereby triggering different recovery mechanisms. To identify the governing forces, the following procedure is used to isolate the force contributions via imbibition experiments conducted under various operational conditions. First, the IFT and CA values are measured as a screening method for the used solutions. Then, the SI efficiency of each system is investigated via an SI test using an Amott cell under ambient conditions, and the dominant force (capillary or gravity) is identified from the recovery profile and oil expulsion front. After that, the FI efficiency of each system is investigated using a modified Amott cell in which various controlled injection pressures can be applied. Finally, the results of these tests are compared by calculating the SI to FI recovery ratio, thereby enabling the dominant force (viscous or capillary) to be identified.

2. MATERIALS AND METHOD

2.1 Materials

Four Bandera Gray sandstone samples (Kocurek Industries, USA), each with diameter of 3.8 cm and a length of around 3.8 cm, were used for the SI and FI recovery experiments. The gas porosity and permeability of the dry core plugs were measured by Nitrogen gas using an AP-680 automated permeameter porosimeter (Coretest Systems Inc., US) under a minimum overburden pressure of 500 psi, and the results are presented in **Table 1**. Bandera Gray mineralogy presented in **Table 2** was obtained by X-ray diffraction (XRD) recorded with a PANalytical X'Pert Pro Multi-purpose Diffractometer using Fe filtered Co K radiation, automatic divergence slit, 2° anti-scatter slit and fast X'Celerator Si strip detector. The diffraction patterns were recorded from 3 to 80° in steps of 0.017° 2 theta with a 0.5 second counting time per step for an overall counting time of approximately 35 minutes.
Qualitative analysis was performed on the XRD data using in-house XPLOT and HighScore Plus (from PANalytical) search/match software. Quantitative analysis was performed on the XRD data using the commercial package TOPAS from Bruker AXT. The results are normalised to 100%, and hence do not include estimates of unidentified or amorphous materials. The pore size distribution of the Bandera Gray sandstone was analyzed via Nuclear Magnetic Resonance (NMR) spectroscopy using a 2.33 MHz GeoSpec II from Oxford Instruments (UK). The sample was saturated with tap water under air vacuum and 1800 psi hydrostatic pressure. The tested sample reached 100% saturation as the water volume intake after saturation is matching the pore volume measured by gas porosimetry. The pore size distribution is presented in **Fig. 1** and records a tri-modal distribution with a dominant population of medium size pore centred at $T_2 \sim 90$ ms; followed by a population of small pores at $T_2 \sim 5$ ms and a minor population of very small pore sizes with $T_2 < 0.1$ ms (limit of the machine sensitivity). Assuming a surface relaxivity dominated by quartz at $r_{T2} \sim 9.3$ μm/s, consistent with literature-reported values for quartz sandstones **(Lucas-Oliveira et al., 2020)**, the relaxation time T_2 can be converted into absolute pore size radius as described by Kleinberg et al. **(Kleinberg et al., 1994)**, Eq. (1):

$$\frac{1}{T_2} = \rho_{T2}\left(\frac{S}{V}\right) \cong \frac{P_G}{r} \tag{1}$$

Where S / V is the ratio of pore surface to pore volume (in μm^{-1}), r is the pore radius (in μm) and P_G is the pore geometry such as P_G= 3 for a sphere and decreases when the aspect ratio of the sphere changes toward a flat cigar shape. As a first approximation, T_2 = 1 ms is equivalent to ~ 0.03 μm pore radius which corresponds to a pore diameter around 5 μm for the dominant population from the NMR distribution. A polarization microscope (Leica DM750 P) was used to capture an image of the rock sample, which is shown in **Fig. 2**.

An Iraqi crude oil was used for the present study. The SARA analysis (IFP 142) of the crude oil resulted in saturate, aromatic, resin and asphaltene fractions of 23.1, 23.0, 14.8 and 39.2 wt%, respectively, with a colloidal instability index, CII = (Saturates + Asphaltenes)/(Aromatics + Resins) ≈ 1.65, which is classified as colloidally unstable (CII > 0.9) indicating strong tendency towards asphaltene aggregation and surface adsorption **(Ashoori et al., 2017)**. The Total Acid Number (TAN, ASTM D664) was 0.4729 mg KOH/g. The Amott water index has been reported to decrease exponentially with increasing TAN of crude oil for acid volcanic reservoir rock from strongly water-wet (Iw = 0.95 at TAN = 0.18 mg KOH/g) to oil-wet (Iw = 0.06–0.11 at TAN = 2.09 mg KOH/g) **(Xie et al., 2010)**. This relationship is valid for a different lithology, but it is consistent with the overall trend of an increase in the tendency to be less water-wet with increasing acidity of crude oil components.

For the surfactants, sodium lauryl sulfate (SLS; Thomas Baker Chemicals, Mumbai-India) and cetyltrimethylammonium bromide (CTAB; Avonchem Limited, Macclesfield-UK) were used. The chemical structures and charge states of each surfactant are shown in **Table 3**. SLS and CTAB are common anionic and cationic surfactants, respectively, that have been extensively studied for their ability to modify the interfacial properties and wettability in enhanced oil recovery (EOR) and multiphase flow applications **(Chowdhury et al., 2022; Kamal et al., 2017; Salehi et al., 2008)**. The liquid and surfactant solutions used for the recovery experiments are presented in **Table 4**.

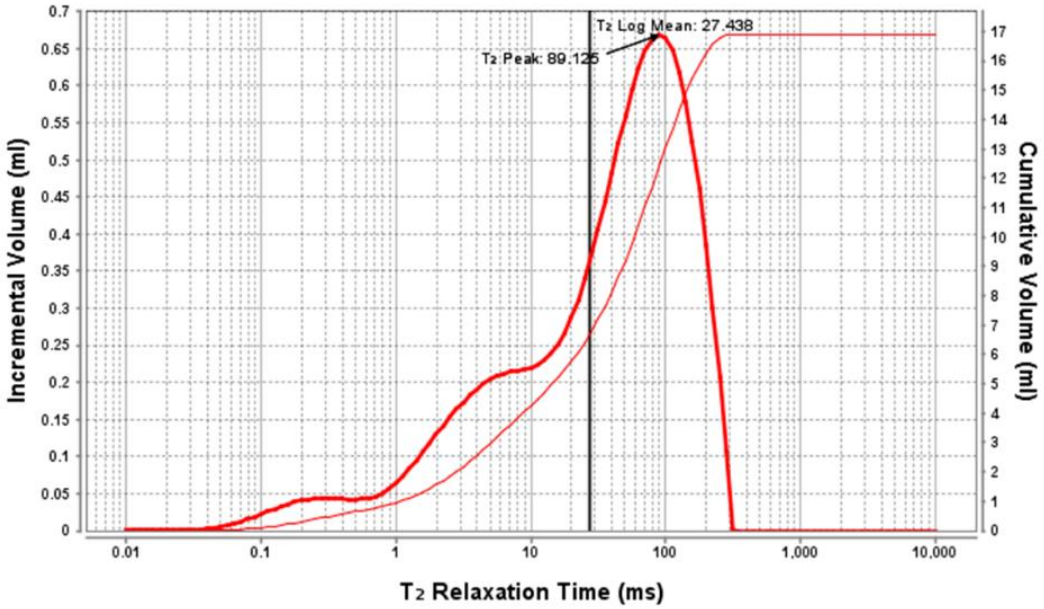


Figure 1. The pore size distribution of the Bandera Gray sandstone, as obtained via NMR

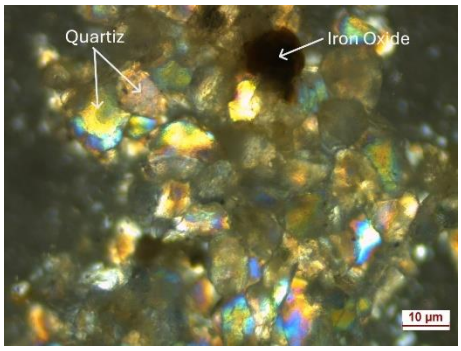


Figure 2. A polarization microscope image of the Bandera Gray sandstone

Table 1. The petrophysical properties of the core samples

Sample #	Length (cm)	Diameter (cm)	Permeability (mD)	Porosity (%)	Pore volume (cc)
1	4	3.8	18.3	19.30	8.83
2	3.3	3.8	19.1	18.10	7.29
3	3.6	3.8	19.5	18.95	7.95
4	3.7	3.8	18.6	19.10	8.12

Table 2. The mineralogy of the Bandera Gray sandstone

Mineral group	Phase	Weight (%)
Silicates	Quartz	57.7
	Albite (a plagioclase feldspar)	18.8
	Microcline (a potassium feldspar)	1.3
	Total	77.8
Clay	Kaolin/Kaolinite	5.4
	Illite/Muscovite	10.2
	Chlorite	2.5
	Total	18.1
Carbonate	Dolomite	3.9
	Calcite	0.2
	Total	4.1

Table 3. The chemical structures and ionic charges of the surfactants used in this study.

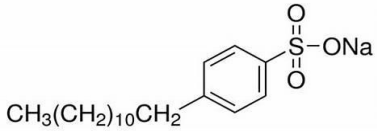
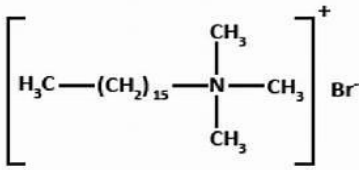
Surfactant	Ionic charge
Sodium lauryl sulfate (SLS) 	Anionic
Cetyltrimethylammonium bromide (CTAB) 	Cationic

Table 4. The solutions used in this study

Solution	Abbreviation
3.5% NaCl	HS (high salinity)
0.5% NaCl	LS (low salinity)
3.5% NaCl + 0.01% CTAB	HS+CTAB
3.5% NaCl + 0.01% SLS	HS+SLS

In this study, a synthetic brine made of only NaCl was used instead of a multi-ion, formation-representative brine with divalent cations (Ca^{2+}, Mg^{2+}). This was intentional so that the effect of salinity and surfactant type on the interfacial tension and contact angle and the resulting SI/FI force balance could be separated from the additional confounding effects of divalent ions. It is known that high concentrations of divalent ions are harmful to the performance of anionic surfactants like SLS, causing precipitation and decreasing the effectiveness of the surfactant **(Shi et al., 2021)**. It is recognized that this is a simplified system compared to actual multi-ion reservoir formation brine, and that further development of the present diagnostic framework in more complex brine chemistries is recommended as a future direction. A high-salinity brine (3.5 wt% NaCl) representative of typical formation/produced water was chosen as the baseline condition instead of a low-salinity brine (e.g., 0.5 wt% NaCl); the four fluid systems investigated were designed to produce a distinct range of interfacial tension and wettability states, and the differential effect of these fluid systems on spontaneous and forced imbibition recovery was used diagnostically to identify the dominant force regime governing each mechanism, which 0.5 wt% NaCl alone would not produce. Low-salinity waterflooding is, however, often constrained in practice by the availability of a suitable low-salinity water source, associated treatment requirements, and additional project costs; the use of surfactants in addition to the original high salinity formation brine is therefore a practical alternative to interfacial and wettability modification in reservoirs where dedicated low-salinity water injection is not readily available.

2.2 Oil-Water IFT Measurements

The IFT between crude oil and various brines was measured using the pendant drop technique, in which a droplet of crude oil was carefully suspended from the tip of a needle submerged in the brine phase **(Eslahati et al., 2020; Sari et al., 2020)**. The droplet profile was captured using a high-resolution camera (UI-3140CP-C-HQ Rev.2, IDS Imaging Development Systems GmbH, Obersulm–Germany), and its shape was analyzed based on the balance between gravitational and interfacial forces. By fitting the droplet outline to the Young–Laplace equation **(Berry et al., 2015; Maldonado-Valderrama et al., 2015; Saad et al., 2011)**(Section 2.4), the IFT was determined with high precision. This technique is particularly suitable for crude oil–brine systems, as it allows accurate measurements under static conditions and minimizes any disturbance to the oil–water interface **(Belghazdis and Hachem, 2025; Zhang et al., 2022)**. Measurements were conducted for crude oil in contact with the HS brine, LS brine, and surfactant-modified HS brines (HS+CTAB and HS+SLS) to evaluate the influence of salinity and chemical additives on the interfacial properties.

2.3 Contact Angle (CA) Measurements

The CA between crude oil, brine, and the rock surface was measured using the sessile drop technique **(Sari et al., 2020)**. For this procedure, polished slices of reservoir rock were first saturated with crude oil to simulate reservoir conditions, after which a droplet of brine was carefully placed on the oil-wet rock surface. Images of the three-phase contact line were captured using a high-resolution camera (UI-3140CP-C-HQ Rev.2, IDS Imaging Development Systems GmbH, Obersulm–Germany). The CA value was then determined by analyzing the droplet profile by axisymmetric fitting to the Young–Laplace equation**(Kwok et al., 1997; Stalder et al., 2010)** (Section 2.4). Measurements were performed for the HS, LS, HS+CTAB, and HS+SLS brines to assess the influence of salinity and surfactant chemistry on wettability alteration. At the 1 minute time point, measurements were not at full equilibrium, and contact angle continued to change for several more minutes in all four fluid systems, especially in the case of HS+CTAB. The 1-minute value was chosen as a standard comparison time to minimize evaporation and exposure artifacts from the extended droplet measurement, and to be conservative with respect to the wettability alteration caused by the surfactant-containing systems, because the eventual water-wet state is greater than captured at 1 minute.

2.4 Spontaneous Imbibition (SI) Experiment

To investigate and distinguish the dominant forces responsible for oil recovery, beyond those acting in flooding experiments (where both viscous and capillary forces are involved), SI experiments were conducted by soaking oil-saturated samples in the test solutions using standard Amott cells **(Amott, 1959)**, as shown in **Fig. 3a**. In this case, the expelled oil is expected to result primarily from natural water imbibition driven by capillary and gravity forces.

2.5 Oil Saturation

The four core samples (**Table 1**) were cleaned with toluene followed by methanol to remove residual hydrocarbons, dried in an oven for 24 h, and then left to cool. The initial weight of each sample was recorded. The samples were then placed in a saturation chamber and fully submerged in crude oil. Here, it should be noted that the rock samples were saturated with oil without any water in order to minimize any errors in calculating the oil saturation volume**(Xu et al., 2019)**. Next, the sample chamber was placed under vacuum (-14.7 psi) and the rocks remained under oil saturation for 30 days. Finally, the core samples were removed, wiped to remove any excess surface oil, and their final weights recorded in order to calculate the oil saturation. The mass of the sample was determined by a balance having a readability of 0.0001 g, which was calibrated before use with a calibration weight supplied by the manufacturer.

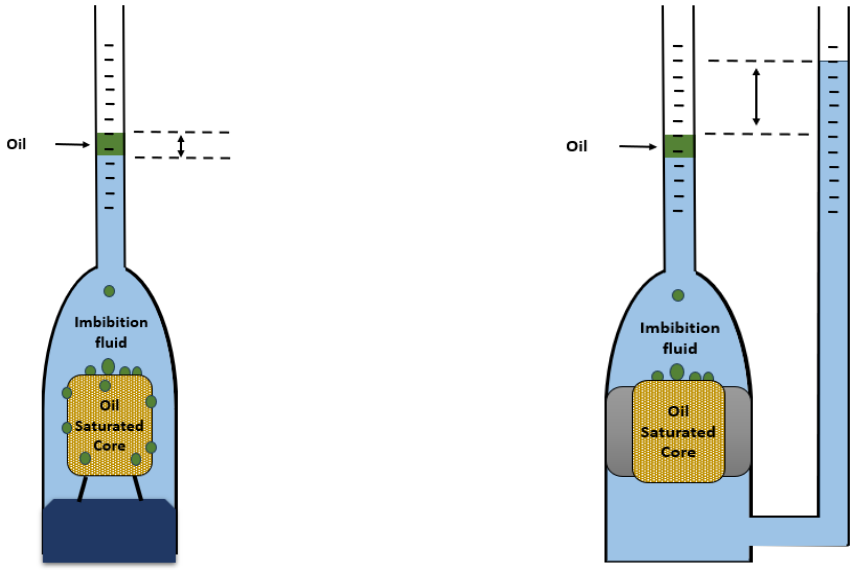
1) For this experiment, four Amott cells were prepared, as shown in **Fig. 3a**, each containing one of the four solutions (**Table 4**) and one oil-soaked sample. All samples were tested simultaneously to ensure they were exposed to identical ambient conditions. To avoid cross-contamination, the Amott cells were cleaned between samples by sequential rinsing with toluene, ethanol and acetone, followed by air drying to remove residual oil and salt.
2) The volume of oil expelled from each rock, which accumulated at the top of the graduated cylinder due to gravity, was recorded daily in order to calculate the cumulative oil

recovery. A high-resolution digital camera (Nikon D5600, Nikon Corporation, Tokyo-Japan) was used to monitor the rock samples and identify the rock surfaces from which oil droplets were expelled.

2.6 Forced Imbibition (FI) Experiment

To further explore the displacement efficiency of each fluid system, an FI experiment was conducted to determine the minimum pressure required to displace oil from the porous media. It was hypothesized that, due to reduced capillary resistance and lower viscous force requirements, the fluid with the lowest IFT (i.e., that forming the smallest oil droplets) would require the lowest pressure head to mobilize the trapped oil **(Khosravani et al., 2024; Leverett, 1941; Wang et al., 2025)**. This experiment makes it possible to compare the resistance to flow imposed by different displacing fluids under the influence of both capillary and applied pressure forces. The protocol is as follows:

1) For this experiment, four modified Amott cells were prepared, as shown in **Fig. 3b**, each containing one of the four solutions (**Table 4**) and a freshly-prepared oil-saturated sample.



a b

Figure 3. The experimental setups for (a) the spontaneous imbibition (SI) experiment and (b) the forced imbibition (FI) experiment.

2) The displacing fluid was forced to flow by applying a pressure head using an elevated fluid reservoir connected to the base of the core sample, with the displaced fluid collected in a graduated tube placed at the top of the core **(Fig. 3b)** and the applied head is the difference in fluid levels between the reservoir and the collection tube. Heads of 10, 20 and 30 cm were sequentially applied to each core, with the head maintained at each stage until oil production stopped, after which the head was increased to the next level; if no oil production occurred at a given stage, the head was raised to the next stage. The head stage at which oil production was first observed is defined as the minimum pressure required to initiate oil production. The volume of expelled oil from each rock sample was recorded in order to calculate the cumulative oil recovery.

Because of the long monitoring time per test (up to 31 days per fluid system) and the need to use freshly-prepared cores to prevent wettability effects from one fluid to another, each

fluid system was tested with only one core sample. In addition to the fluid systems compared, minor variations in core porosity and permeability **(Table 1)** are also recognized as a potential source of variation.

2.7 Capillary Pressure Circulation

The capillary pressure (P_C) is the pressure required for a non-wetting fluid (e.g., gas or oil) to displace a wetting fluid (e.g., water) in a porous medium **(Alipour and Sakhaee-Pour, 2023; Li et al., 2022; Sahu and Yadav, 2023)**. The P_C increases with the increase in IFT, decrease in contact angle (increase in water-wettability), and decrease in pore size. In drainage, a high P_C resists displacement of the wetting phase; in imbibition, it enhances the displacement of the non-wetting phase. Therefore, to further quantify the results, the P_C is calculated by using Eq. (2) **(Cai et al., 2022)**:

$$P_C = P_{nw} - P_w \quad (2)$$

where P_{nw} is the pressure of the non-wetting phase, and P_w is the pressure of the wetting phase.

In terms of a simplified model, the Young-Laplace equation can express the P_C as a function of the oil-water IFT and the water/oil-rock CA, as shown in Eq. (3) **(Alipour and Sakhaee-Pour, 2023; Sari et al., 2020)**:

$$P_C = \frac{2 * IFT * \cos CA}{r} \quad (3)$$

where r is the radius of the capillary. For simplicity, the average pore radius for all samples was assumed to be constant. The average pore radius of 2.5 μm, which corresponds to the dominant pore population identified by NMR **(Fig. 1)**, was applied to all samples; all cores are from the same source rock, so this value is assumed to be representative, and r is assumed to be constant across fluid systems, so it does not affect the relative Pc comparison used for force-regime classification.

3. RESULTS AND DISCUSSION

3.1 Oil-Water IFT

The measured IFT values between crude oil and the various injection fluids are compared in **Fig. 4**. Here, the highest IFT of 5.9 mN/m is observed for the HS brine, while the lowest IFT (1.2 mN/m) is observed for the HS+CTAB system. Both surfactant-containing solutions are found to significantly reduce the IFT compared to the brine-only systems. Thus, overall, the IFT values increase in the order: HS+CTAB (1.2 mN/m) < HS+SLS (2.9 mN/m) < LS (4.3 mN/m) < HS (5.9 mN/m).

The lower IFT in the presence of the LS fluid compared to the HS fluid clearly reflects the influence of ionic strength in governing oil–water interfacial behavior **(Kakati and Sangwai, 2017; Moeini et al., 2014; Rostami et al., 2019)**. Under low-salinity conditions, the reduced concentration of dissolved ions weakens electrostatic screening and expands the electrical double layer at the interface, which enhances interfacial interactions and promotes IFT reduction.

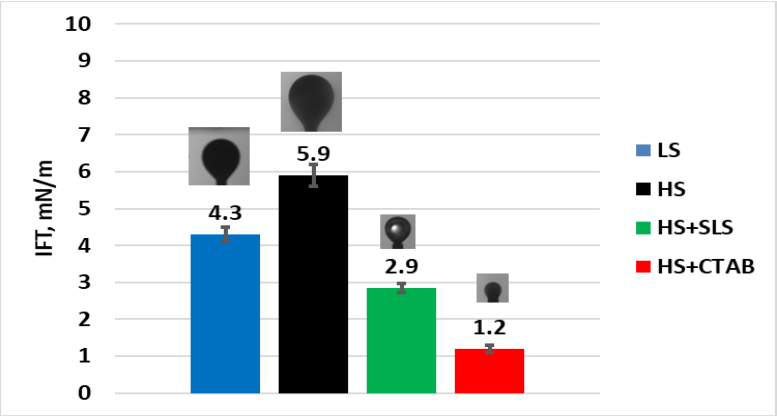


Figure 4.. The oil-water interfacial tension (IFT) values of the various injection fluids (error bars = standard deviation).

Conversely, high-salinity conditions compress the electrical double layer and stabilize the interface, resulting in relatively higher IFT values **(Aziz et al., 2019; Snosy et al., 2020; Wen et al., 2017)**. Meanwhile, the surfactant-containing solutions provide further reductions in the IFT due to the adsorption and orientation of surfactant molecules at the oil–water interface **(Nowrouzi et al., 2020; Yekeen et al., 2020)**. Their hydrophilic heads orient toward the aqueous phase and hydrophobic tails toward the oil phase. This preferential adsorption disrupts intermolecular cohesive forces at the interface and lowers the interfacial free energy. Together, these mechanisms highlight the combined effects of salinity tuning and surfactant action in enhancing interfacial modification, which is essential for improving oil mobilization in CEOR processes **(Dey et al., 2025; Xue et al., 2025)**. The critical micelle concentration (CMC) of anionic surfactants like SLS is known to decrease with increasing electrolyte concentration, which is due to the screening of electrostatic repulsion between charged head groups by ionic strength. This could lead to micellization at lower surfactant concentrations, which would decrease the amount of SLS available for interfacial adsorption compared to bulk micelles, and is consistent with the relatively small decrease in IFT found for HS+SLS compared to HS+CTAB.

3.2 Contact Angle (CA) Measurements

The measured CA values of the injected fluid droplets on oil-saturated rock slices over time are presented in **Table 5**, while the CA values after 1 min (when stabilization has been reached) are compared graphically in **Fig. 5**. Here, the HS brine exhibits an intermediate-wet state (CA = 78.3°) and is used as the baseline. By comparison, the LS fluid exhibits a slightly increased water-wetness **(Salehi et al., 2008)**, although the rock remains intermediate-wet (CA = 73.5°). By contrast, each surfactant-containing solution induces a strong shift toward water-wet conditions, regardless of the ionic type. Moreover, the SLS produces the most pronounced effect, achieving a contact angle of 0° within 1 min. Overall, the CA increases in the order: HS (78.3°) < LS (73.5°) < HS + CTAB (22.5°) < HS + SLS (0°). This ordering is consistent with the mechanistic difference between anionic and cationic surfactants reported in the literature whereby anionic surfactants like SLS can effects wettability by solubilizing micelles of adsorbed hydrophobic components and reducing intermolecular forces at the rock surface **(Kamal et al., 2017; Xu et al., 2019)**, and cationic surfactants like CTAB do so by ion-pair formation between the positively charged surfactant head and negatively charged carboxylates adsorbed on the rock **(Deng et al., 2021)**.However, in clay-rich sandstone, the high surface area and negative charge of clay minerals like kaolinite and

illite **(Table 2)** favor competitive adsorption of CTAB onto the clay surfaces **(Sohal et al., 2016; Kamal et al., 2017)**, and this is likely to reduce the effective surfactant concentration available to wettability modification at the oil-rock interface and accounts for the relatively incomplete wettability alteration (CA = 22.5 0) in spite of the large IFT reduction seen with this system. IFT reduction and the resulting shift in wettability (as determined by the contact angle) are the most important factors in determining the SI-to-FI transition observed in this study, but the crude's colloidally unstable character (CII ≈ 1.65) also provides compositional context for the transition, consistent with a baseline tendency toward wettability alteration, and does not explain the differences observed between fluid systems.

Table 5. The average contact angle (CA) measurements ((round 1+2+3)/3) of each solution as a function of time

Time (min)	LS	HS	HS+CTAB	HS+SLS
0	86.3	85.2	43.1	20.95
1	73.5	78.3	22.5	0
2	69.25	73.45	5.5	0
3	63.5	69.25	0	0
4	60.35	66	0	0
5	57.5	63.6	0	0

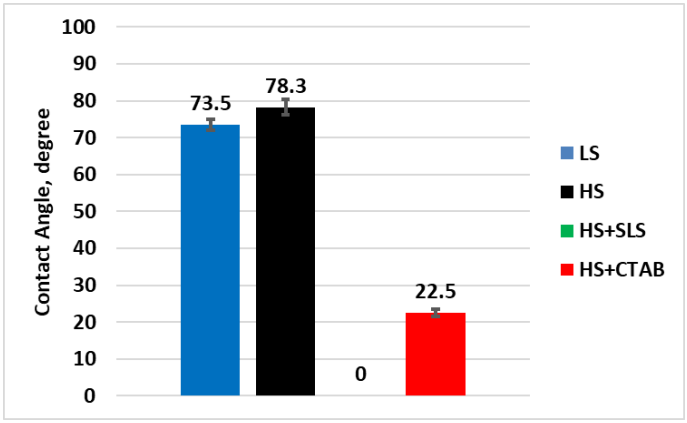


Figure 5. The average contact angles of the various oil-water-rock systems after 1 min (error bars = standard deviation).

3.3 Spontaneous Imbibition Recovery (Capillary/Gravity-Driven Recovery)

3.3.1 The Oil Recovery–Time Profiles

The oil recovery–time profiles obtained from the SI experiments for the four solutions are presented in **Fig. 6**. Here, the ultimate oil recovery is seen to decrease in the order: HS+SLS (41.0%) > LS (34.5%) > HS (34.3%) > HS+CTAB (5.0%). Further, the recovery profiles can be divided into three distinct stages. In the early stage, oil recovery increases rapidly and almost linearly, being governed primarily by capillary forces. During the middle stage, however, the recovery rate slows and becomes nonlinear, thereby reflecting the coupled action of capillary and gravity forces. Finally, in the late stage, oil recovery approaches a plateau, with gravity-driven imbibition emerging as the dominant mechanism. The absence of one or more of these regions when deploying certain fluids is attributed to variations in rock properties, fluid characteristics, and pressure conditions **(Deng et al., 2021; Rostami Ravari et al., 2011; Singh and Mohanty, 2016)**. This three-stage behavior is generally in line with the recovery regimes as reported by **(Rostami Ravari et al., 2011)** in the oil-wet

carbonate cores, where capillary-, combined-, and gravity-dominated stages were also reported **(Rostami Ravari et al., 2011)**. It is important to note, however, that the proportion of the gravity-driven stage in the current sandstone system is significantly lower than the values that have been reported in the case of carbonate systems **(Rostami Ravari et al., 2011)**, which is explained by the fact that the permeability of the Bandera Gray sandstone (approximately 19 mD) is significantly lower than that of the limestone cores in the latter case (approximately 364 mD). This dependence of gravity drainage on permeability is in line with the findings of **(Deng et al., 2021)** who observed that the forces of gravity become dominant over the forces of capillarity with an increase in permeability **(Deng et al., 2021)**.

For the HS and LS solutions, the recovery profiles exhibit all three stages, with approximately 25% recovery in the early stage (capillary action), nearly 30% recovery in the middle stage (combined capillary and gravity forces), and 32.5% and 35% recovery for the HS and LS, respectively, in the late stage. Conversely, the recovery profiles of the HS+SLS and HS+CTAB solutions only display the middle and late stages. Moreover, the HS+SLS exhibits no clear recovery during the early stage, with recovery beginning in the middle stage, where it is driven by both capillary and gravity mechanisms. By contrast, the HS+CTAB shows minimal recovery even during the middle stage, and reaches only 5% recovery during the late (gravity-driven) stage. This exceptionally low spontaneous recovery of the CTAB system, even with its high wettability change (CA = 22.5 o) and lowest measured IFT (1.2 mN/m) is a direct confirmation of the theoretical forecast of **(Deng et al., 2021)**, who proved that ultralow IFT inhibits capillary-driven imbibition in systems that have been shifted to water-wet conditions by decreasing the positive capillary pressure that would have otherwise driven counter-current imbibition **(Deng et al., 2021)**. Experimentally, a similar coupling effect was observed by **(Xu et al., 2019)** in low-permeability sandstone, where too much reduction of the IFT was found to reduce the capillary driving force caused by the change in wettability, leading to recovery behavior dominated by gravity and not by the capillary imbibition. The current findings can be used to generalize these results to a clay-enriched sandstone system and to validate that the IFT capillary pressure trade-off is a controlling factor in the performance of CEOR that cannot be determined solely by IFT or CA measurements.

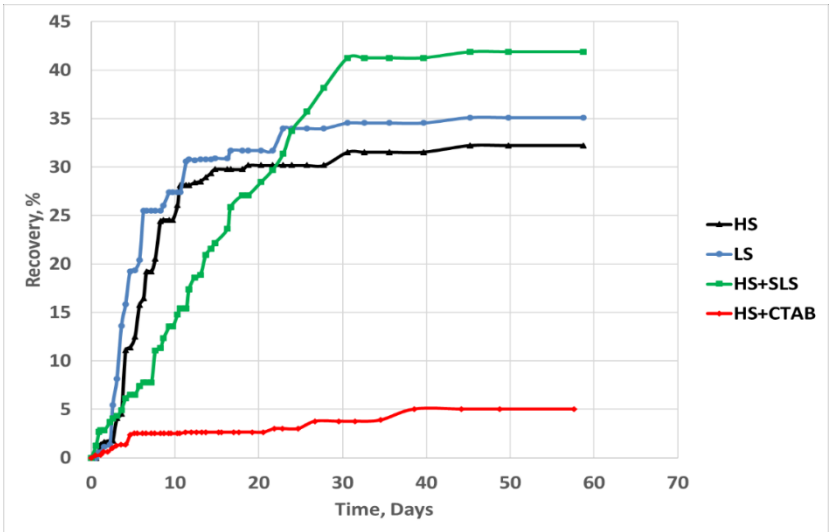


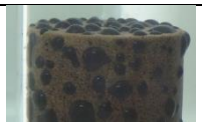
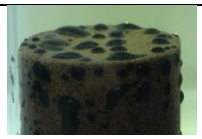
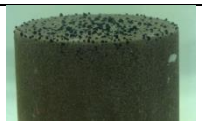
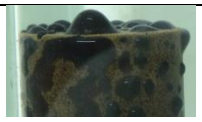
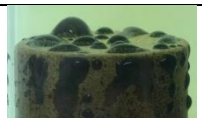
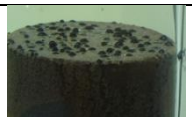
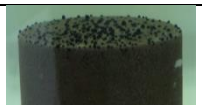
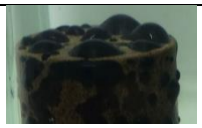
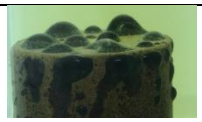
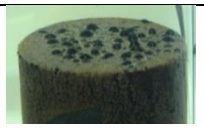
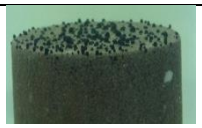
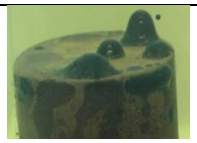
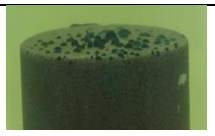
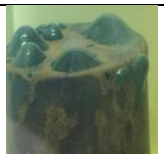
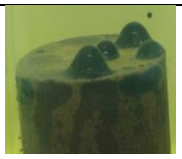
Figure 6. The time-dependent recovery (%) during spontaneous imbibition for each solution

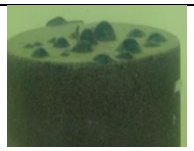
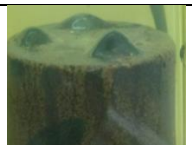
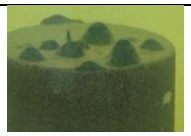
3.3.2 Correlation between Oil Expulsion Pattern and the Forces Governing Recovery

The sequential images of the core samples during the SI experiments are presented in **Table 6**. The primary purpose of this experiment was to observe the pattern and behavior of oil expulsion from the core surfaces in the SI process. The results indicate that the chemical composition of the soaking solution significantly affects the pattern and behavior of the oil produced. Thus, although similar oil production patterns are observed for the samples immersed in the LS, HS, and HS+SLS solutions, the production rates and volumes are seen to differ. Specifically, the samples immersed in LS and HS produce oil across the entire core surface, with oil droplets gradually enlarging and detaching over time. Similarly, in the HS+SLS solution, oil appears on all sides, but at a slower rate and volume, with visibly smaller droplets. Conversely, in the HS+CTAB solution, oil is mainly produced from the top of the sample, and at a much slower rate compared to the other solutions, and these droplets remain small throughout the experiment.

The spatial and temporal patterns of oil expulsion from the samples provide direct insight into the dominant driving forces governing the recovery process. The occurrence of oil expulsion across all surfaces suggests a synergistic contribution of capillary and gravity forces, as evident in the LS, HS, and HS+SLS cases. By contrast, expulsion that is limited to the top surface alone signifies gravity-controlled recovery, which is associated with the diminished production rate seen in the HS+CTAB **(Deng et al., 2021; Gupta et al., 2020; You et al., 2018)**.

Table 6. The images of the core samples when soaked in the various fluids for the SI process.

Day	LS	HS	SLS	CTAB
1				
2				
3				
6				
14				
22				

25				
32				
44				

3.3.3 Correlation between Oil Recovery and Oil Expulsion Pattern

As outlined in section 3.3.2, the oïl expulsion patterns in **Table 6** reflect the forces governing the recovery process and are expected to correlate with the overall recovery performance. For the HS, LS, and HS+SLS solutions, the patterns indicate that recovery is driven by the combined influence of capillary and gravity forces. In the case of the HS+CTAB, however, recovery is dominated by gravity alone. This mechanistic distinction is consistent with the spontaneous imbibition results in **Fig. 6** (Section 3.3.1), which show high recoveries for the HS, LS, and HS+SLS (due to the synergistic action of capillary and gravity forces) and substantially lower recovery for the gravity-dominated HS+CTAB case. Similar distinctions have been noted in the literature, where it has been reported that an ultra-low IFT in water-wet rocks can suppress recovery by diminishing the capillary pressure **(Deng et al., 2023b; Deng et al., 2021; Rostami Ravari et al., 2011; Wang et al., 2011; You et al., 2018)**. Accordingly, recovery in the HS+CTAB system appears to be governed primarily by gravity, which is consistent with the recovery–time profile and the observation that oil is expelled only from the top surface. This gravity-dominated mechanism explains the poor spontaneous imbibition performance, despite the favorable wettability and IFT conditions.

Capillary pressure

The above quantitative IFT, CA, and oil recovery results are compared with the calculated capillary pressure (P_c) values in **Table 7**. Here, the recovery is seen to decrease with decreasing P_c. These results confirm that the capillary pressure, which is influenced by both the CA and IFT, is the primary driving force during the SI process.

Table 7. A comparison between the calculated capillary pressure (P_c) values and the measured IFT, CA, and recovery for the various solutions

Solution	IFT (Nm)	CA (°)	Pc (Pa)	Rel. P_C (%)	Recovery (%)	Rel. Recovery (%)
HS	0.0059	78	981	43.0	32	78.0
LS	0.0043	73	1006	44.1	35	85.4
HS+SLS	0.00285	0	2280	100 (Ref)	41	100 (Ref)
HS+CTAB	0.0012	23	884	38.8	5	12.2

"Ref" indicates the reference system used for normalization. Rel. PC (%) = Capillary pressure normalized to the highest PC value in the dataset (HS+SLS = 100%). Rel. Recovery (%) = Oil recovery normalized to the highest recovery value (HS+SLS = 100%).

In brief, despite achieving an ultra-low IFT, the HS+CTAB system underperforms relative to the other solutions, indicating a markedly weaker contribution of capillary forces during the spontaneous imbibition (SI) recovery process **(Alvarez and Schechter, 2017; Mason and Morrow, 2013)**. Under such conditions, the excessive reduction in IFT diminishes capillary pressure, thereby limiting the driving force for counter-current imbibition and shifting the dominant recovery mechanism toward gravity drainage. These findings clearly demonstrate that strong water-wetness combined with a moderately reduced IFT is more favorable for efficient SI recovery than an ultra-low IFT alone **(Cai et al., 2020)**. This highlights the critical balance between wettability and interfacial tension in controlling capillary-driven oil displacement during CEOR processes.

3.4 Forced Imbibition Recovery (Capillary/Viscous Driven Recovery)

To gain a deeper insight into the dominant driving mechanisms of oil recovery and the mobilization of trapped oil, a series of FI experiments was performed using a modified Amott cell. This setup enabled controlled displacement under an applied pressure gradient, thus making it possible to distinguish the relative contributions of capillary, gravity, and viscous forces during forced oil displacement. The time-dependent FI oil recovery profiles of the four displacing solutions at applied pressure heads of 10, 20, and 30 cm are presented in **Fig. 7**. Here, the ultimate oil recovery is seen to decrease in the order: HS+CTAB (56%) > HS+SLS (53%) > LS (51%) > HS (49%). Thus, the FI recovery trends of the HS and LS brines (**Fig. 7**), which exhibit moderate capillary forces, are comparable with those observed during SI (**Fig. 6**). Moreover, while these samples exhibit relatively low ultimate FI recoveries of 49.0% and 51%, respectively, compared to 53% and 56% for HS+SLS and HS+CTAB, respectively, these recoveries are achieved over a comparatively short duration of ~9.8 days. Moreover, both brine systems require a maximum pressure head of 30 cm before the onset of oil production, thereby indicating that the generated capillary pressure is insufficient to initiate flow without an additional viscous input. This suggests that while the capillary force is active, it is not strong enough to sustain continued oil displacement, so that the entry of the displacing fluid into the pore throats must be assisted by viscous pressure **(Li et al., 2017; Malenica et al., 2024)**.

Meanwhile, despite their differing SI behaviors (**Fig. 6**), the HS+CTAB and HS+SLS systems each exhibit noticeably higher final recoveries of 56% and 53%, respectively, during forced displacement (**Fig. 7**). In particular, the HS+CTAB solution, which exhibited a low capillary pressure during SI (thereby causing spontaneous gravity-driven expulsion), starts to produce oil under FI only when a pressure head of 20 cm is applied. The recovery then plateaus at 55.34% at 15.7 days, while a higher-pressure head of 30 cm pushes the ultimate recovery to 56.36% after 17 days, which represents the highest recovery among all four systems. Meanwhile, the HS+SLS system, which generates the highest P_c during the SI process (**Table 7**), begins producing oil at the lowest pressure head of 10 cm during FI (**Fig. 7**), which clearly indicates a lower viscous entry threshold. This confirms that the FI process in the HS+SLS case involves capillary-assisted viscous displacement, where capillary pressure supports viscous flow rather than opposing it. As a result, the recovery reaches 50% at 22 days, while higher pressure heads of 20 and 30 cm lead to further boosts in recovery, reaching 51.35% (27 days) and 52.7% (31 days), respectively. Although the HS+SLS system does not reach the same peak recovery as the HS+CTAB within the same timeframe, it requires considerably less applied pressure to mobilize the oil. Overall, the surfactant-containing systems (HS+SLS and HS+CTAB), which generate lower

IFT values (**Table 7**), produce smaller and more deformable droplets than the HS and LS systems, thereby enhancing their ability to pass through pore throats once the viscous force is applied. In other words, a low IFT reduces the interfacial resistance, promotes oil–water phase rearrangement, and facilitates droplet movement under viscous flow **(Alshehri and Kovscek, 2016; Schechter et al., 1991; Schechter et al., 1994)**. As a result, the surfactant-containing solutions require less viscous energy input to initiate oil mobilization compared to the simple brines **(Chowdhury et al., 2022)**. However, despite having the lowest IFT, the HS+CTAB solution still requires a higher pressure head (20 cm) to initiate production compared to the HS+SLS (10 cm). This indicates that IFT alone does not dictate entry behavior. This finding has important practical significance: it demonstrates that the minimum viscous force required to initiate oil mobilization is governed by the combined capillary pressure of the system rather than by IFT alone, and that a fluid capable of generating high capillary pressure through aggressive wettability alteration — even at a moderate IFT — can outperform a fluid with ultralow IFT but weaker wettability modification under forced displacement conditions. To the best of the authors' knowledge, this relationship between entry pressure threshold and the combined IFT–wettability state has not been quantified experimentally in the CEOR literature using a controlled low-pressure gravity-head apparatus of the type employed here.

Moreover, the stronger water-wet condition induced by the HS+SLS (CA ≈ 0°), reduces the adhesion forces between the oil and rock, thereby lowering the displacement energy barrier. This generates a higher capillary pressure during SI (**Table 7**), and continues to assist displacement even during FI. By contrast, the HS+CTAB generates a low capillary pressure during SI, thereby resulting in an initial gravity-dominated expulsion stage, while a viscous-dominated regime is achieved only upon the application of pressure. This suggests that the HS+SLS system operates via a capillary-assisted viscous mechanism, whereas the HS+CTAB system behaves as a gravity-to-viscous transition system under FI. Therefore, while the IFT defines the droplet deformability, it is the combination of IFT and wettability-induced capillary pressure that governs the viscous entry threshold.

In brief: (i) the HS and LS brines each exhibit a moderate P_c and viscous-assisted FI, (ii) the HS+SLS exhibits a high P_c and capillary-assisted viscous FI, and (iii) the HS+CTAB exhibits a very low P_c, with gravity-driven SI and viscous-dominated FI. These force interactions are further validated in the following section by using the SI/FI ratio as a diagnostic indicator of force dominance.

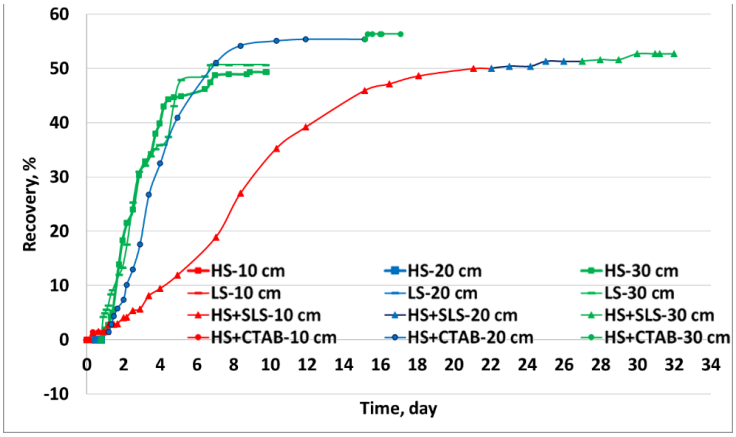


Figure 7. The time-dependent recovery (%) for each solution during forced imbibition (FI) at various applied pressures

3.5 Explaining the Interplay Between the Various Driving Forces in Oïl Recovery

Given that recovery during FI is influenced by both capillary and viscous forces, a comparative interpretation of the force contributions can be obtained by using the spontaneous-to-forced imbibition (SI/FI) recovery ratio, as proposed in the literature **(Aslanidis et al., 2022; Liu et al., 2025)**. A similar SI/FI comparison was used by **(Liu et al., 2025)** in tight oil reservoirs and were found to report that SI/FI ratios greater than 60 percent represent capillary dominated displacement and those less than 20 percent represent viscous dominated displacement with intermediate values representing a transitional regime. These thresholds are widely consistent with the current results: the HS and LS systems yield SI/FI ratios of 65–69%, placing them in the capillary-assisted viscous regime; the HS+SLS system yields ~80%, confirming strong capillary dominance; and the HS+CTAB system yields ~9%, indicating near-complete viscous dominance. Significantly, however, this diagnostic method is further expanded by the current study in that the SI/FI ratio is directly correlated with measured IFT, CA, and calculated capillary pressure values of each fluid system and, as such, offers a more mechanistically based interpretation than ratio-based classification alone. The force contribution zones are shown graphically in **Fig. 8**, while the recovery regimes are classified based on the SI/FI response in **Table 8**. Thus, a high SI/FI ratio indicates a strong capillary contribution during FI, while a low ratio suggests that viscous forces are dominant. Therefore, the SI/FI ratio serves as a validation tool to confirm the force regimes inferred from Section 3.4. For instance, the HS and LS exhibit 32% and 35% recoveries due to moderate capillary and minor gravity forces during SI, compared to 49% and 51%, respectively, during FI. This leads to SI/FI ratios of 65–69%, which indicates that while the capillary force continues to contribute significantly during forced recovery, viscous support is needed in order to sustain displacement. This is consistent with the viscous-assisted capillary regime inferred above. The relatively high pressure requirement (30 cm) further supports the conclusion that simple brine systems generate limited capillary pressure, thereby necessitating an external viscous force to push water into the pore throats and mobilize the residual oil.

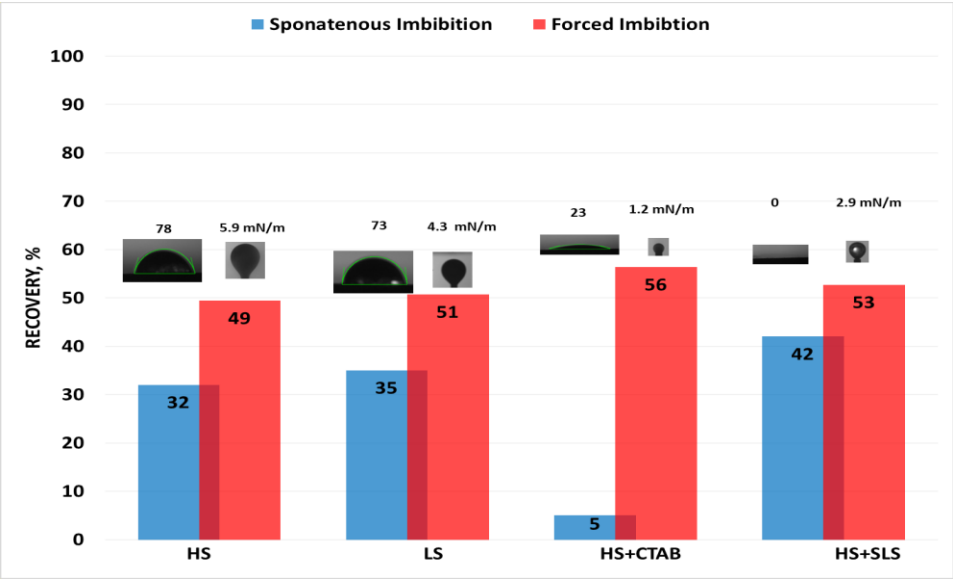


Figure 8. The oil recovery statistics of the various solutions during different recovery conditions (SI or FI).

The thresholds were developed for a matrix–fracture soaking model in tight oil reservoirs, which has a much lower permeability than the Bandera Gray sandstone used here (18–20 mD; **Table 1**). The SI/FI ratio is not specifically limited to a particular permeability class, but the numerical values have not been independently tested in conventional sandstone systems and this is a limitation. The regime assignments for these are also consistent with the independently measured IFT, CA and calculated Pc trends **(Table 7).**

In the presence of CTAB, the recovery during SI is limited (5%) and is primarily gravity driven, as the capillary pressure is extremely low (the IFT is too low and there is insufficient wettability alteration). During FI, however, the recovery increases sharply to 56%, thus yielding a low SI/FI ratio of ~9%. This confirms that the viscous force becomes the dominant driving mechanism in FI, replacing the gravity-driven expulsion observed in SI.In the presence of SLS, the spontaneous recovery (42%) reflects strong capillary-driven displacement due to a high P_c (low IFT + strong water-wetness). During FI, the recovery is increased to 53% at a pressure head of only 10 cm, thus resulting in a high SI/FI ratio of ~80%. This confirms that the HS+SLS system maintains capillary dominance even under forced conditions, thus resulting in capillary-assisted viscous displacement.

Table 8. A summary of the force regime classification

System	SI Mechanism	FI Mechanism	SI/FI ratio →	Force regime
HS or LS	Capillary driven	Viscous-assisted capillary	65–69%	Moderate P_c → Viscous-assisted capillary (i.e. Capillary active but needs viscous support
HS+SLS	Strong capillary	Capillary-assisted viscous	~80%	High P_c → Capillary-assisted viscous (i.e. Strong capillary sustained under pressure
HS+CTAB	Gravity driven	Viscous dominated	~9%	Low P_c → Gravity-to-viscous transition (Capillary negligible)

4. CONCLUSIONS

Conventional CEOR evaluation relies heavily on IFT and CA measurements correlated with core flooding or spontaneous imbibition results individually, an approach that fails to isolate the relative contributions of capillary, viscous, and gravity forces and therefore cannot reliably explain why low IFT does not always translate into improved recovery. The present study addressed this gap by introducing a force-isolation diagnostic workflow applied to clay-rich Bandera Gray sandstone, combining spontaneous imbibition (SI), low-pressure forced imbibition (FI) using a modified Amott cell capable of identifying the minimum entry pressure required to mobilize trapped oil, and SI/FI ratio analysis, all linked quantitatively to measured IFT, contact angle (CA), and calculated capillary pressure. The following conclusions were drawn:

It is important to note that the force regimes mentioned below are not measured, but rather inferred from recovery profiles, oil-expulsion observations, and the SI/FI ratio.

- Simple high-salinity (HS) and low-salinity (LS) brines show moderate capillary-driven spontaneous recovery, but require high viscous input to initiate flow during FI, thereby

indicating a viscous-assisted capillary regime rather than purely viscous or capillary-dominated recovery.

- The addition of an anionic surfactant (sodium lauryl sulfate, SLS) is associated with the highest calculated capillary pressure and strongest water-wetness, thereby resulting in rapid SI and capillary-assisted viscous FI in which capillary and viscous forces act cooperatively. This system mobilizes oil at the lowest applied pressure.
- The use of a cationic surfactant (cetyltrimethylammonium bromide, CTAB) is associated with a minimal inferred capillary contribution, thus leading to gravity-driven SI. However, this transitions to a viscous-dominant regime during FI, as the external pressure replaces gravity as the primary driving force. This classification is based on the combined evidence of a small calculated capillary pressure and a negligible SI recovery (5%) for this system, and not on the magnitude of the calculated capillary pressure alone; the subsequent FI/SI ratio (~9%) is also an independent indication of the viscous dominance of the forced imbibition process. It is also important to note that the applied head of 10 cm is not a precisely resolved minimum entry pressure, but rather the lowest pressure stage tested at which oil production was first observed, which was not measured at finer resolution in this study.
- The SI/FI ratio effectively validates the inferred force regimes, thereby demonstrating that capillary force can either assist or require viscous support, or be bypassed entirely, depending on the interfacial condition induced by the chemical system.
- These findings confirm that fluid design for CEOR should be guided by force regime classification rather than IFT reduction alone, as the IFT and CA only translate to recovery when the resulting capillary pressure is sufficient to influence displacement under both SI and FI conditions.

Overall, the proposed force-deconstruction workflow provides a clearer mechanistic basis for evaluating CEOR systems and can help to resolve inconsistencies in the literature, where IFT and CA trends can fail to correlate with the oil recovery performance.

NOMENCLATURE

Symbol	Description	Symbol	Description
CA	Contact angle (°)	*Pw*	Pressure of the wetting phase (Pa)
CEOR	Chemical enhanced oil recovery	*r*	Capillary / pore radius (μm)
CTAB	Cetyltrimethylammonium bromide	*S/V*	Pore surface-to-volume ratio (μm^{-1})
EOR	Enhanced oil recovery	*SI*	Spontaneous imbibition
FI	Forced imbibition	*SLS*	Sodium lauryl sulfate
HS	High-salinity brine	*T2*	Transverse (spin–spin) relaxation time (ms)
IFT	Interfacial tension (mN/m)	*WA*	Wettability alteration
k	Permeability (mD)	*XRD*	X-ray diffraction
LS	Low-salinity brine	*ρ*	Surface relaxivity (μm/s)
NMR	Nuclear magnetic resonance	*c*	capillary (as in Pc)
P	Pressure (Pa)	*G*	geometry (as in PG)
Pc	Capillary pressure (Pa)	*nw*	non-wetting phase (as in Pnw)
PG	Pore geometry factor	*w*	wetting phase (as in Pw)
Pnw	Pressure of the non-wetting phase (Pa)	*2*	transverse relaxation (as in T2)

Credit Authorship Contribution Statement

Faaiz Al-Shajalee: Writing – original draft, Methodology, Investigation, Formal analysis, Software. Hussein H. Hussein: Methodology, Investigation, Formal analysis, Software. Ahmad Sari: Writing -review & editing, Methodology. Lionel Estban: Writing -review & editing, Methodology. Haider A. Falih Al-Tarim: Methodology, Investigation. Nurudeen Yekeen: Writing -review & editing.

Declaration of Competing Interest

The authors declare that they have no known financial or personal relationships that could have appeared to influence the work reported in this paper.

REFERENCES

Al-Anssari, S., Ali, M., Alajmi, M., Akhondzadeh, H., Khaksar Manshad, A., Kalantariasl, A., Iglauer, S., and Keshavarz, A., 2021. Synergistic effect of nanoparticles and polymers on the rheological properties of injection fluids: implications for enhanced oil recovery. *Energy & Fuels*, 35(7), pp. 6125-6135. https://doi.org/10.1021/acs.energyfuels.1c00105.

Al-Anssari, S., Arain, Z.U.A., Barifcani, A., Keshavarz, A., Ali, M., and Iglauer, S., 2018. Influence of pressure and temperature on CO2-nanofluid interfacial tension: Implication for enhanced oil recovery and carbon geosequestration. *In Abu Dhabi International Petroleum Exhibition & Conference.*. https://doi.org/10.2118/192964-MS. *OnePetro*.

Al-Shajalee, F., Al-Obaidi, D.A., Abed, A.A., Machale, J., Al-Shalabi, E.W., Arif, M., Badi, D., Wood, C., and Saeedi, A., 2025. Shear thickening behaviour of cross-linked polyacrylamide gels induced by gas flow in porous media. *Arabian Journal for Science and Engineering*, pp. 1-11. https://doi.org/10.1007/s13369-025-10639-3.

Ali, M., Al-Anssari, S., Shakeel, M., Arif, M., Dahraj, N.U., Iglauer, S., 2017. Influence of miscible CO 2 Flooding on wettability and asphaltene precipitation in Indiana lime stone. *In SPE/IATMI Asia Pacific Oil & Gas Conference and Exhibition.* https://doi.org/10.2118/186204-MS.

Ali, M., Dahraj, N.U., and Haider, S.A., 2015. Study of asphaltene precipitation during CO2 injection in light oil reservoirs. *In SPE/PAPG Pakistan section Annual Technical Conference.* https://doi.org/10.2118/181130-MS.

Alipour, M., and Sakhaee-Pour, A., 2023. Application of Young-Laplace with size-dependent contact angle and interfacial tension in shale. *Geoenergy Science and Engineering*, 231, P. 212447. https://doi.org/10.1016/j.geoen.2023.212447.

Alshehri, A.J., and Kovscek, A.R., 2016. In-situ visualization of multidimensional imbibition in dual-porosity carbonates. *SPE Journal*, 21(05), pp. 1631-1642. https://doi.org/10.2118/170811-PA.

Alvarez, J.O., and Schechter, D.S., 2017. Wettability alteration and spontaneous imbibition in unconventional liquid reservoirs by surfactant additives. *SPE Reservoir Evaluation & Engineering*, 20(01), pp. 107-117. https://doi.org/10.2118/177057-PA.

Amott, E., 1959. Observations relating to the wettability of porous rock. *Transactions of the AIME*, 216(01), pp. 156-162. https://doi.org/10.2118/1167-G.

Ashoori, S., Sharifi, M., Masoumi, M., and Mohammad Salehi, M., 2017. The relationship between SARA fractions and crude oil stability. *Egyptian Journal of Petroleum*, 26(1), pp. 209-213. https://doi.org/10.1016/j.ejpe.2016.04.002.

Aslanidis, P., Strand, S., Puntervold, T., Yeboah, K.K., and Souayeh, I., 2022. Oil recovery by low-rate waterflooding in water-wet sandstone cores. *In SPE Europec featured at EAGE Conference and Exhibition?,* P. D041S013R005. https://doi.org/10.2118/209688-MS.

Awan, M.M.A., and Kirmani, F.U.D., 2025. CO2 injection for enhanced oil recovery: Analyzing the effect of injection rate and bottom hole pressure. *Petroleum Research*, 10(1), pp. 129-136. https://doi.org/10.1016/j.ptlrs.2024.08.006.

Azad, M.S. 2021. IFT role on oil recovery during surfactant based EOR methods. *Surfactants in Upstream E&P*. Springer. pp. 115-148. https://doi.org/10.1007/978-3-030-70026-3_4

Aziz, R., Joekar-Niasar, V., Martínez-Ferrer, P.J., Godinez-Brizuela, O.E., Theodoropoulos, C., and Mahani, H., 2019. Novel insights into pore-scale dynamics of wettability alteration during low salinity waterflooding. *Scientific Reports*, 9(1), P. 9257. https://doi.org/10.1038/s41598-019-45434-2.

Belghazdis, M., and Hachem, E.K., 2025. In-depth exploration of interfacial tension measurement techniques: an updated review. *Matériaux & Techniques*, 113(3), P. 302. https://doi.org/10.1051/mattech/2025015.

Berry, J.D., Neeson, M.J., Dagastine, R.R., Chan, D.Y., and Tabor, R.F., 2015. Measurement of surface and interfacial tension using pendant drop tensiometry. *Journal of Colloid and Interface Science*, 454, pp. 226-237. https://doi.org/10.1016/j.jcis.2015.05.012.

Cai, J., Chen, Y., Qiao, J., Yang, L., Zeng, J., and Sun, C., 2022. Determination of dynamic capillary effect on two-phase flow in porous media: A perspective from various methods. *Petroleum Science*, 19(4), pp. 1641-1652. https://doi.org/10.1016/j.petsci.2022.01.017

Cai, J., Li, C., Song, K., Zou, S., Yang, Z., Shen, Y., Meng, Q., and Liu, Y., 2020. The influence of salinity and mineral components on spontaneous imbibition in tight sandstone. *Fuel*, 269, P. 117087. https://doi.org/10.1016/j.fuel.2020.117087.

Chai, M., Chen, Z., Nourozieh, H., Yang, M., Xu, J., Sun, Z., and Li, Z., 2024. Perspectives of dimethyl ether (DME) as a transitional solvent for enhanced oil recovery (EOR). *Energy*, 310, P. 133191. https://doi.org/10.1016/j.energy.2024.133191.

Chaturvedi, K.R., Pandey, A., and Sharma, T. 2024. Viability of EOR when oil prices are low. *Advancements in Chemical Enhanced Oil Recovery*. Apple Academic Press. pp. 25-37. https://doi.org/10.1201/9781003453727-2

Chowdhury, S., Shrivastava, S., Kakati, A., and Sangwai, J.S., 2022. Comprehensive review on the role of surfactants in the chemical enhanced oil recovery process. *Industrial & Engineering Chemistry Research*, 61(1), pp. 21-64. https://doi.org/10.1021/acs.iecr.1c03301.

Dashtaki, S.R.M., Ali, J.A., Manshad, A.K., Nowrouzi, I., Mohammadi, A.H., and Keshavarz, A., 2020. Experimental investigation of the effect of Vitagnus plant extract on enhanced oil recovery process using interfacial tension (IFT) reduction and wettability alteration mechanisms. *Journal of Petroleum Exploration and Production Technology*, 10(7), pp. 2895-2905. https://doi.org/10.1007/s13202-020-00966-6.

Deng, X., Kamal, M.S., Patil, S., Hussain, S.M.S., Mahmoud, M., Al-Shehri, D., and Al-Shalabi, E.W., 2023a. Investigation of the coupled effect of IFT reduction and wettability alteration for oil recovery: New insights. *ACS Omega*, 8(13), pp. 12069-12078. https://doi.org/10.1021/acsomega.2c07906.

Deng, X., Patil, S., Al Shehri, D., Kamal, M.S., Shakil, S.M., Zhou, X., Mahmoud, M., Al Shalabi, E.W., and Hassan, A., 2023b. IFT reduction negatively impacts oil recovery when wettability alteration happens. *In SPE Gas & Oil Technology Showcase and Conference.* P. D031S047R003. https://doi.org/10.2118/214178-MS.

Deng, X., Tariq, Z., Murtaza, M., Patil, S., Mahmoud, M., and Kamal, M.S., 2021. Relative contribution of wettability Alteration and interfacial tension reduction in EOR: A critical review. *Journal of Molecular Liquids*, 325, P. 115175. https://doi.org/10.1016/j.molliq.2020.115175.

Dey, S., Khan, M.A., Prakash, S., Jangid, L., Joshi, D., and Mandal, A., 2025. Synthesis and physicochemical evaluation of an olive oil-derived anionic surfactant: effects on interfacial tension, wettability alteration, and oil recovery efficiency. *Industrial & Engineering Chemistry Research*, 64(33), pp. 16375-16392. https://doi.org/10.1021/acs.iecr.5c00323.

Eslahati, M., Mehrabianfar, P., Isari, A.A., Bahraminejad, H., Manshad, A.K., and Keshavarz, A., 2020. Experimental investigation of Alfalfa natural surfactant and synergistic effects of Ca2+, Mg2+, and SO42− ions for EOR applications: Interfacial tension optimization, wettability alteration and imbibition studies. *Journal of Molecular Liquids*, 310, P. 113123. https://doi.org/10.1016/j.molliq.2020.113123.

Fattahi, R., Lashkarbolooki, M., Abedini, R., and Younesi, H., 2023. Investigating the synergistic/antagonistic effects of mixing SiO2 nanoparticles and ionic liquid, nonionic emulsifier, and gemini surfactants on the main mechanisms of crude oil production. *Energy & Fuels*, 37(19), pp. 14741-14751. https://doi.org/10.1021/acs.energyfuels.3c02569.

Gupta, I., Rai, C.S., and Sondergeld, C.H., 2020. Impact of surfactants on hydrocarbon mobility in shales. *SPE Reservoir Evaluation & Engineering*, 23(03), pp. 1105-1117. https://doi.org/10.2118/201110-PA.

Haghighi, O.M., Zargar, G., Khaksar Manshad, A., Ali, M., Takassi, M.A., Ali, J.A., and Keshavarz, A., 2020. Effect of environment-friendly non-ionic surfactant on interfacial tension reduction and wettability alteration; implications for enhanced oil recovery. *Energies*, 13(15), pp. 3988. https://doi.org/10.3390/en13153988.

Hosseini, E., Hajivand, F., and Tahmasebi, R., 2019. The effect of alkaline–surfactant on the wettability, relative permeability and oil recovery of carbonate reservoir rock: experimental investigation. *Journal of Petroleum Exploration and Production Technology*, 9(4), pp. 2877-2891. https://doi.org/10.1007/s13202-019-0671-4.

Jha, N.K., Ali, M., Iglauer, S., Lebedev, M., Roshan, H., Barifcani, A., Sangwai, J.S., and Sarmadivaleh, M., 2019. Wettability alteration of quartz surface by low-salinity surfactant nanofluids at high-pressure and high-temperature conditions. *Energy & Fuels*, 33(8), pp. 7062-7068. https://doi.org/10.1021/acs.energyfuels.9b01102.

Kakati, A., and Sangwai, J.S., 2017. Effect of monovalent and divalent salts on the interfacial tension of pure hydrocarbon-brine systems relevant for low salinity water flooding. *Journal of Petroleum Science and Engineering*, 157, pp. 1106-1114. https://doi.org/10.1016/j.petrol.2017.08.017.

Kamal, M.S., Hussein, I.A., and Sultan, A.S., 2017. Review on surfactant flooding: phase behavior, retention, IFT, and field applications. *Energy & Fuels*, 31(8), pp. 7701-7720. https://doi.org/10.1021/acs.energyfuels.7b00353.

Khosravani, M., Akhlaghi, N., and Hosseini, S., 2024. Investigation of ionic liquid adsorption and interfacial tension reduction using different crude oils; effects of salts, ionic liquid, and pH. *Scientific Reports*, 14(1), P. 10720. https://doi.org/10.1038/s41598-024-58458-0.

Kleinberg, R., Kenyon, W., and Mitra, P., 1994. Mechanism of NMR relaxation of fluids in rock. *Journal of Magnetic Resonance, Series A*, 108(2), pp. 206-214. https://doi.org/10.1006/jmra.1994.1112.

Kwok, D., Gietzelt, T., Grundke, K., Jacobasch, H.J., and Neumann, A.W., 1997. Contact angle measurements and contact angle interpretation. 1. Contact angle measurements by axisymmetric drop shape analysis and a goniometer sessile drop technique. *Langmuir*, 13(10), pp. 2880-2894. https://doi.org/10.1021/la9608021.

Leverett, M., 1941. Capillary behavior in porous solids. *Transactions of the AIME*, 142(01), pp. 152-169. https://doi.org/10.2118/941152-G.

Li, S., Ding, Y.H., Cai, B., Lu, Y., and Gu, D., 2017. Solution for counter-current imbibition of 1D immiscible two-phase flow in tight oil reservoir. *Journal of Petroleum Exploration and Production Technology*, 7(3), pp. 727-733. https://doi.org/10.1007/s13202-016-0273-3.

Li, Y., Liu, C., Li, H., Chen, S., Lu, K., Zhang, Q., and Luo, H., 2022. A review on measurement of the dynamic effect in capillary pressure. *Journal of Petroleum Science and Engineering*, 208, P. 109672. https://doi.org/10.1016/j.petrol.2021.109672.

Liu, Z., Xu, L., Wu, S., Ding, H., Gong, H., Zhao, H., Sun, H., and Dong, M., 2025. Quantitative characterization of spontaneous and forced imbibition during soaking process in tight oil reservoirs. *Journal of Dispersion Science and Technology*, pp. 1-20. https://doi.org/10.1080/01932691.2025.2462697.

Lucas-Oliveira, E., Araujo-Ferreira, A.G., Trevizan, W.A., dos Santos, B.C.C., and Bonagamba, T.J., 2020. Sandstone surface relaxivity determined by NMR T2 distribution and digital rock simulation for permeability evaluation. *Journal of Petroleum Science and Engineering*, 193, P. 107400. https://doi.org/10.1016/j.petrol.2020.107400.

Maldonado-Valderrama, J., Torcello-Gómez, A., del Castillo-Santaella, T., Holgado-Terriza, J.A., and Cabrerizo-Vílchez, M.A., 2015. Subphase exchange experiments with the pendant drop technique. *Advances in Colloid and Interface Science*, 222, pp. 488-501. https://doi.org/10.1016/j.cis.2014.08.002.

Malenica, L., Zhang, Z., and Angst, U., 2024. Towards improved understanding of spontaneous imbibition into dry porous media using pore-scale direct numerical simulations. *Advances in Water Resources*, 194, P. 104840. https://doi.org/10.1016/j.advwatres.2024.104840.

Mason, G., and Morrow, N.R., 2013. Developments in spontaneous imbibition and possibilities for future work. *Journal of Petroleum Science and Engineering*, 110, pp. 268-293. https://doi.org/10.1016/j.petrol.2013.08.018.

Moeini, F., Hemmati-Sarapardeh, A., Ghazanfari, M.-H., Masihi, M., and Ayatollahi, S., 2014. Toward mechanistic understanding of heavy crude oil/brine interfacial tension: The roles of salinity, temperature and pressure. *Fluid Phase Equilibria*, 375, pp. 191-200. https://doi.org/10.1016/j.fluid.2014.04.017.

Nowrouzi, I., Mohammadi, A.H., and Manshad, A.K., 2020. Water-oil interfacial tension (IFT) reduction and wettability alteration in surfactant flooding process using extracted saponin from Anabasis Setifera plant. *Journal of Petroleum Science and Engineering*, 189, P. 106901. https://doi.org/10.1016/j.petrol.2019.106901.

Rahevar, S., Kakati, A., Kumar, G., Sangwai, J., Myers, M., and Al-Yaseri, A., 2023. Controlled salinity water flooding and zeta potential: Insight into a novel enhanced oil recovery mechanism. *Energy Reports*, 9, pp. 2557-2565. https://doi.org/10.1016/j.egyr.2023.01.088.

Rostami, P., Mehraban, M.F., Sharifi, M., Dejam, M., and Ayatollahi, S., 2019. Effect of water salinity on oil/brine interfacial behaviour during low salinity waterflooding: A mechanistic study. *Petroleum*, 5(4), pp. 367-374. https://doi.org/10.1016/j.petlm.2019.03.005.

Rostami Ravari, R., Strand, S., and Austad, T., 2011. Combined surfactant-enhanced gravity drainage (SEGD) of oil and the wettability alteration in carbonates: the effect of rock permeability and interfacial tension (IFT). *Energy & Fuels*, 25(5), pp. 2083-2088. https://doi.org/10.1021/ef200085t.

Saad, S.M., Policova, Z., and Neumann, A.W., 2011. Design and accuracy of pendant drop methods for surface tension measurement. *Colloids and Surfaces A: Physicochemical and Engineering Aspects*, 384(1-3), pp. 442-452. https://doi.org/10.1016/j.colsurfa.2011.05.002.

Sahu, N., and Yadav, S.R., 2023. Fluid flow through porous medium including dynamic capillary pressure: a review with mathematical aspects. *In International Conference on Computational Modeling and Sustainable Energy*. pp. 431-443. https://doi.org/10.1007/978-981-97-6794-6_27. *Springer*.

Salehi, M., Johnson, S.J., and Liang, J.T., 2008. Mechanistic study of wettability alteration using surfactants with applications in naturally fractured reservoirs. *Langmuir*, 24(24), pp. 14099-14107. https://doi.org/10.1021/la802464u.

Sari, A., Al Maskari, N.S., Saeedi, A., and Xie, Q., 2020. Impact of surface roughness on wettability of oil-brine-calcite system at sub-pore scale. *Journal of Molecular Liquids*, 299, P. 112107. https://doi.org/10.1016/j.molliq.2019.112107.

Schechter, D., Zhou, D., and Orr Jr, F., 1991. Capillary imbibition and gravity segregation in low IFT systems. *In SPE Annual Technical Conference and Exhibition?,* pp. SPE-22594-MS. https://doi.org/10.2118/22594-MS.

Schechter, D., Zhou, D., and Orr Jr, F., 1994. Low IFT drainage and imbibition. *Journal of Petroleum Science and Engineering*, 11(4), pp. 283-300. https://doi.org/10.1016/0920-4105(94)90047-7.

Shi, Y., Miller, C., and Mohanty, K., 2021. Surfactant-aided low-salinity waterflooding for low-temperature carbonate reservoirs. *SPE Journal*, 26(04), pp. 2214-2230. https://doi.org/10.2118/201754-PA.

Singh, R., and Mohanty, K.K., 2016. Foams with wettability-altering capabilities for oil-wet carbonates: a synergistic approach. *SPE Journal*, 21(04), pp. 1126-1139. https://doi.org/10.2118/175027-PA.

Snosy, M.F., Abu El Ela, M., El-Banbi, A., and Sayyouh, H., 2020. Comprehensive investigation of low-salinity waterflooding in sandstone reservoirs. *Journal of Petroleum Exploration and Production Technology*, 10(5), pp. 2019-2034. https://doi.org/10.1007/s13202-020-00862-z.

Sohal, M.A., Thyne, G., and Søgaard, E.G., 2016. Review of recovery mechanisms of ionically modified waterflood in carbonate reservoirs. *Energy & Fuels*, 30(3), pp. 1904-1914. https://doi.org/10.1021/acs.energyfuels.5b02749.

Stalder, A.F., Melchior, T., Müller, M., Sage, D., Blu, T., and Unser, M., 2010. Low-bond axisymmetric drop shape analysis for surface tension and contact angle measurements of sessile drops. *Colloids and Surfaces A: Physicochemical and Engineering Aspects*, 364(1-3), pp. 72-81. https://doi.org/10.1016/j.colsurfa.2010.04.040.

Wang, J., Hu, Y., Chu, X., Sun, G., and Lu, T., 2025. Roles and thresholds of viscosity and interfacial tension in surfactant flooding for residual oil recovery. *Frontiers in Chemistry*, 13, P. 1660041. https://doi.org/10.3389/fchem.2025.1660041.

Wang, Y., Xu, H., Yu, W., Bai, B., Song, X., and Zhang, J., 2011. Surfactant induced reservoir wettability alteration: Recent theoretical and experimental advances in enhanced oil recovery. *Petroleum Science*, 8(4), pp. 463-476. https://doi.org/10.1007/s12182-011-0164-7.

Wen, B., Sun, C., Bai, B., Gatapova, E.Y., and Kabov, O.A., 2017. Ionic hydration-induced evolution of decane–water interfacial tension. *Physical Chemistry Chemical Physics*, 19(22), pp. 14606-14614. https://doi.org/10.1039/C7CP01826F.

Xie, Q., He, S., and Pu, W., 2010. The effects of temperature and acid number of crude oil on the wettability of acid volcanic reservoir rock from the Hailar Oilfield. *Petroleum Science*, 7(1), pp. 93-99. https://doi.org/10.1007/s12182-010-0011-2.

Xu, D., Bai, B., Wu, H., Hou, J., Meng, Z., Sun, R., Li, Z., Lu, Y., and Kang, W., 2019. Mechanisms of imbibition enhanced oil recovery in low permeability reservoirs: Effect of IFT reduction and wettability alteration. *Fuel*, 244, pp. 110-119. https://doi.org/10.1016/j.fuel.2019.01.118.

Xue, Y., He, C., Bai, Y., Jiang, W., He, L., and Sui, H., 2025. Interfacially active components in heavy oil: structure, interfacial behaviors, and regulation strategies. *ChemPlusChem*, 90(7), P. e202500064. https://doi.org/10.1002/cplu.202500064.

Yekeen, N., Malik, A.A., Idris, A.K., Reepei, N.I., and Ganie, K., 2020. Foaming properties, wettability alteration and interfacial tension reduction by saponin extracted from soapnut (Sapindus Mukorossi) at room and reservoir conditions. *Journal of Petroleum Science and Engineering*, 195, P. 107591. https://doi.org/10.1016/j.petrol.2020.107591.

You, Q., Wang, H., Zhang, Y., Liu, Y., Fang, J., and Dai, C., 2018. Experimental study on spontaneous imbibition of recycled fracturing flow-back fluid to enhance oil recovery in low permeability sandstone reservoirs. *Journal of Petroleum Science and Engineering*, 166, pp. 375-380. https://doi.org/10.1016/j.petrol.2018.03.058.

Zhang, K., Georgiadis, A., and Trusler, J.M., 2022. Measurements and interpretation of crude Oil-Water/Brine dynamic interfacial tension at subsurface representative conditions. *Fuel*, 315, P. 123266. https://doi.org/10.1016/j.fuel.2022.123266.

Zhang, Z., Azad, M.S., and Trivedi, J., 2021. IFT or wettability alteration: What is more important for oil recovery in oil-wet formation? *Fuel*, 291, P. 119986. https://doi.org/10.1016/j.fuel.2020.119986.

التداخل بين التوتر السطحي البيني وتبللية الصخور وانتقال أنظمة القوى على الاستخلاص الكيميائي المحسّن للنفط: منهجية تشخيصية آلية قائمة على نسبة الاستخلاص بين الامتصاص التلقائي و الامتصاص القسري

فائز الشجالي[1]، [*]، حسين هادي حسين[2]، احمد ساري[3]، ليونيل استبان[4]، حيدر احمد فالح الطريم[5]، نورالدين ياكين[6]

[1]قسم هندسة النفط، كلية الهندسة، جامعة كركوك، كركوك، العراق

[2] قسم هندسة النفط، كلية الهندسة، جامعة بغداد، بغداد، العراق

[3] مونادلفوس، منطقة التعدين والمعادن في الشمال الغربي، بيرث، أستراليا الغربية، أستراليا.

[4] منظمة الكومنولث للبحوث العلمية والصناعية(CSIRO) ، بيرث، أستراليا الغربية، أستراليا.

[5] شركة الاستكشافات النفطية، وزارة النفط، بغداد، العراق.

[6] كلية الهندسة، جامعة ايدث كاون، جوندلاب، غرب استراليا، استراليا.

الخلاصة

على الرغم من الدور المحوري لاستخلاص النفط المعزز (EOR) في تلبية الطلب المتزايد على الطاقة، إلا أن تفسير أداء الاستخلاص الكيميائي المعزز يكون محدودٌ بسبب الاعتماد على بيانات التوتر السطحي وزاوية التلامس. تربط معظم الدراسات التوتر السطحي وزاوية التلامس بنتائج حقن السوائل في اللب، مما يحجب تأثير قوى الشعرية والجاذبية. تقدم هذه الدراسة منهجية لعزل القوى من خلال الاستخلاص المتحكم فيه لتميز بين القوة الشعرية واللزوجة والجاذبية، وذلك من خلال الجمع بين تجارب الامتصاص التلقائي والامتصاص القسري التي أُجريت على عينات لبية من حجر رملي باندیرا غراي غني بالطين. يتمثل الابتكار الرئيسي في خلية أموت المعدلة التي تطبق ضغوطًا هيدروليكية مضبوطة (10–30 سم) أثناء تجربة الامتصاص القسري، مما يسمح بقياس أدنى ضغط لتحفيز إزاحة النفط في كل نظام سائل. تم اختيار أربعة أنظمة حقن (محلول ملحي عالي الملوحة (HS)، ومحلول ملحي منخفض الملوحة(LS) ، ومادة خافضة للتوتر السطحي (أنيونية كبريتات لوريل الصوديوم SLS) ومادة خافضة للتوتر السطحي (كاتيونية بروميد سيتيل تريميثيل الأمونيوم CTAB) لتحفيز ظروف التفاعل البيني. يُولّد محلول SLS ضغطًا شعريًا عاليًا وزاوية تلامس شبه معدومة، مما يُعزز الاستخلاص بالامتصاص القسري (بسبب قوة اللزوجة) مدعوما بالخاصية الشعرية عند أدنى عتبة ضغط، محققًا استخلاص بنسبة 41% (بسبب الامتصاص التلقائي) ونسبة الاستخلاص بواسطة الامتصاص التلقائي الى الاستخلاص بواسطة الامتصاص القسري (SI/FI) تبلغ حوالي 80%. في المقابل، يُنتج بروميد CTAB توترًا بينيًا منخفضًا ولكن ضغطًا شعريًا غير كافٍ، مما يؤدي إلى استخلاص بواسطة الامتصاص التلقائي نتيجة لقوة الجاذبية بنسبة 5% اما الاستخلاص بالامتصاص القسري فيكون نتيجة لقوة اللزوجة، و ونسبة الاستخلاص بواسطة الامتصاص التلقائي الى الاستخلاص بواسطة الامتصاص القسري (SI/FI) تبلغ حوالي 9%. تُظهر أنظمة المحلول الملحي استخلاص بواسطة القوة الشعرية مدعومة بقوة اللزوجة، مما يتطلب أعلى ضغط دخول للمسامات. تُصنّف نسبة (SI/FI) أنظمة القوى، مؤكدةً أن القوة الشعرية تتحكم في حركة السوائل في ظل ظروف الامتصاص التلقائي و الامتصاص القسري. يوفر هذا النهج القائم على أنظمة القوى أساسًا أكثر موثوقية لتصميم تركيبات CEOR مقارنةً بفحص التوتر السطحي وزاوية التلامس وحدهما.

الكلمات المفتاحية: قوة الضغط الشعري، الامتصاص القسري، الشد السطحي، الامتصاص التلقائي، تغير التبللية.